E-band telecom-compatible 40 dB gain high-power bismuth-doped fiber amplifier with record power conversion efficiency

Aleksandr Donodin ✉ 🅘 ; Egor Manuylovich 🅘 ; Vladislav Dvoyrin; Mikhail Melkumov 🅘 ; Valery Mashinsky 🅘 ;
Sergei Turitsyn 🅘

Check for updates

View
Online

Export
Citation

AIP Publishing
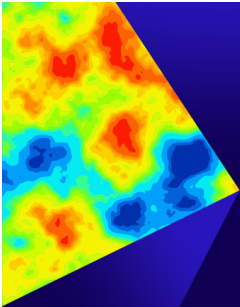
E-band telecom-compatible 40 dB gain high-power bismuth-doped fiber amplifier with record power conversion efficiency

View Online   Export Citation   CrossMark

Aleksandr Donodin,[1,a] Egor Manuylovich,[1] Vladislav Dvoyrin,[1] Mikhail Melkumov,[2]
Valery Mashinsky,[2] and Sergei Turitsyn[1]

AFFILIATIONS

[1] Aston Institute of Photonics Technologies, Aston University, Birmingham, United Kingdom
[2] Prokhorov General Physics, Institute of the Russian Academy of Sciences, Dianov Fiber Optics Research Center Moscow,
Russian Federation

[a] Author to whom correspondence should be addressed: a.donodin@aston.ac.uk

ABSTRACT

Multi-band transmission is one of the key practical solutions to cope with the continuously growing demand on the capacity of optical communication networks without changing the huge existing fiber base. However, ultra-broadband communication requires the development of novel power efficient optical amplifiers operating beyond C- and L-bands, and this is a major research and technical challenge comparable to the introduction of the seminal erbium-doped fiber amplifiers that dramatically changed the optical communication sector. There are several types of optical fibers operating beyond C- and L-bands that can be used for the development of such amplifiers, specifically the fibers doped with neodymium, praseodymium, thulium, and bismuth. However, among these, Bi-doped fibers are of special interest as the most promising amplification medium because, unlike the others, different Bi-associated active centers allow amplification in an enormous band of overall width of 700 nm (1100–1800 nm). Such spectral coverage can be obtained by using different host materials, such as aluminosilicate, phosphosilicate, silica, and germanosilicate glasses. Here, we report a novel Bi-doped fiber amplifier with record characteristics for E-band amplification, including the highest power conversion efficiency among telecom-compatible E-band amplifiers reported to date. This bismuth-doped fiber amplifier (BDFA) features a maximum gain of 39.8 dB and a minimal noise figure of 4.6 dB enabled by 173 m Bi-doped fiber length. The maximum achieved power conversion efficiency of 38% is higher than that of L-band Er-doped fiber amplifiers. This performance demonstrates the high potential of BDFA for becoming the amplifier of choice in modern multi-band optical communication networks.

I. INTRODUCTION

The development of novel approaches to increase the throughput of optical networks to cope with the constantly growing capacity demand is one of the significant challenges in the communication industry.[1] There are three main approaches to meet this demand. The first one focuses on the development of more sophisticated data modulation formats and probabilistic shaping.[2] However, this direction is limited by restrictions on the maximum spectral efficiency imposed by fiber nonlinearity through the nonlinear Shannon limit[3] and the logarithmic scaling of the achievable rates with the linear increase in signal-to-noise ratio (SNR).[3] The second approach

focuses on utilizing spatial division multiplexing (SDM). SDM can be implemented either by using additional standard single-mode fibers (SSFM) (including dark fibers) or through the development of multi-core or multi-mode fiber transmission lines. Although SDM is important in the long term, both of these approaches require substantial changes to the existing infrastructure.[1,4]

The third method to increase the capacity is to utilize the huge, available spectral bandwidth of the existing fiber base through multi-band transmission (MBT),[4] which, unlike SDM, does not require a new fiber deployment. The conventional optical networks exploit a bandwidth of only 10 THz allowed by commercially available Er-doped fiber amplifiers (EDFAs) in C- and L-optical bands

08 April 2024 16:24:09

(1530–1620 nm).[5] The MBT maximizes the return on investments in the existing infrastructures[4] by the transmission in the so-called O, E, S, and U optical bands. However, it requires a substantial advance in efficient optical amplifiers for these spectral bands, similar to a major breakthrough in telecommunications made by the development of Er-doped fiber amplifiers.[6,7]

There exist a number of techniques to achieve amplification beyond the C- and L-bands: Raman amplifiers,[8] semiconductor optical amplifiers (SOAs),[9] fiber optical parametric amplifiers (FOPA),[10] and amplifiers based on active optical fibers, i.e., fibers doped with various chemical elements (mostly, rare-earths). Each technique has specific advantages and drawbacks; solutions can vary across the applications from ultra-long-haul systems to metro and access networks. One of the key specifications for many applications is power efficiency. The amplifiers based on active fibers are a promising solution for MBT as they can be potentially comparable in performance to EDFAs, that is, the amplifier of choice in C- and L-bands. In comparison to other solutions, active fiber amplifiers do not require as much pump power as Raman amplifiers, which is critically important for undersea cables, and are shorter than discrete Raman amplifiers. In comparison to FOPAs, active fiber amplifiers have higher power conversion efficiency (PCE); they achieve higher gain as compared to SOAs and do not have such high nonlinearity and saturation as SOA.[9,11] There are a number of active fiber media operating beyond C- and L-bands, doped with neodymium (Nd),[12] praseodymium (Pr),[13] thulium (Tm),[14] and bismuth (Bi).[15] The unique advantage of bismuth-doped glasses is that Bi-associated active centers in different glass hosts have several broad amplification bands covering most of ~1100–1800 nm.[15–19] Such spectral coverage can be achieved with the use of different host materials, such as aluminosilicate, phosphosilicate, silica, and germanosilicate glasses. Hence, bismuth-doped fibers (BDFs) could be considered as the most promising candidate for MBT applications. The bismuth-doped fiber amplifiers (BDFAs) have shown a great potential for telecommunication applications and expansion of the bandwidth of the conventional transmission systems after successful information transmissions in O-[20,21] and E-bands,[22,23] coherent transmission,[24,25] and the simultaneous signal amplification in different amplification bands.[15,26] An important milestone for BDFAs is to achieve a performance comparable to the EDFAs operating in the C-band.

In this work, we use germanosilicate BDF to develop an amplifier operating in the E-band and to demonstrate a record 40-dB gain with 4.6-dB noise figure (NF). The developed single-stage amplifier features a bandwidth of 80 nm and is based on a single-pass scheme. The performance of the developed amplifier is optimized and experimentally characterized in terms of key parameters such as magnitudes of gain, NF, 3-dB bandwidth, and PCE for different pump and signal powers. Different pumping schemes (PSs) are investigated and optimized, targeting the best achievable key parameters. We would like to stress that the major advancement of our work is not only the highest gain (the optical gain of 38 dB in the E-band BDFA has already been reported[27]) but also the combination of the highest gain, lowest NF, and the superior power conversion efficiency. We demonstrate the record PCE of 38% in the amplifier, which is a critical parameter for utilizing BDFAs in power-efficient multi-band transmission networks.

II. EXPERIMENTAL SETUP

A schematic of the bismuth-doped fiber amplifier is shown in Fig. 1(a). The developed amplifier consists of two thin-film filter wavelength division multiplexers (TFF-WDMs) used for multiplexing and demultiplexing of radiation at the pump (1250–1320 nm) and signal (1330–1500 nm) wavelengths. The TFF-WDMs have very steep and flat transmission and reflection bands that enable consistent loss over the whole operation bandwidth. Two isolators centered at 1320 nm were used to avoid back reflection of radiation to the pump diodes, and two 1440 nm isolators were used for unidirectional transmission of the signal.

The Bi-doped germanosilcate fiber used in this work is fabricated in-house using the conventional all-gas modified chemical vapor deposition (MCVD) doping technique and has a length of 173 m. The fiber has core and cladding diameters of 6 and 125 μm, respectively. The index difference (Δn) between the core and cladding is around 0.007. The fiber core consists of 95 mol % SiO_2, 5 mol % GeO_2, and <0.01 at% of bismuth. The cutoff wavelength (λ_c) of the fiber is measured to be around 1060 nm. The splice loss between SMF and Bi-doped fiber was measured to be 0.5 dB. The bismuth ions stabilized in the silicate glass hosts (various germanosilicate, phosphorosilicate, and aluminosilicate glasses) and associated with the silica glass matrix give rise to the broad absorption and emission bands peaked in the vicinity of 1400 nm.[28–31] The shapes of these absorption and emission bands observed in the investigated fiber closely resemble the characteristic optical absorption and emission spectra that can be found, for instance, in Ref. 29 and Ref. 30, respectively. The optical loss in the investigated fiber is of 0.19 dB/m at the pump wavelength of 1320 nm. The optical loss level at the wavelength of 1550 nm, which is mainly attributed to the passive loss in the fiber, is at the level of 0.02 dB/m.
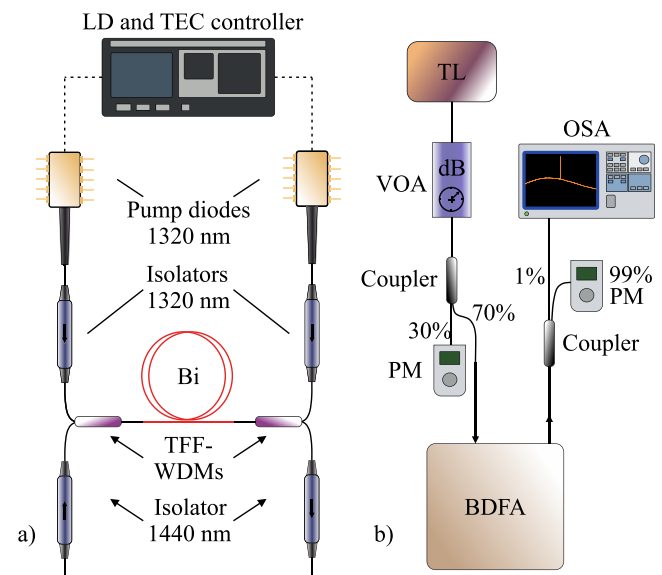

FIG. 1. (a) Schematic bismuth-doped fiber amplifier and (b) schematics of the gain and NF measurements.

The schematic of the setup for the gain and NF measurement is presented in Fig. 1(b). It contains a tunable laser (TL) operating in the 1384–1484 nm wavelength range that is used as an input signal. The power of the input signal is controlled by a variable optical attenuator (VOA). A 70/30 coupler is used to enable the monitoring of the input signal power with a power meter (PM) at the input of the developed BDFA in real time: 30% of the total optical signal is directed to the PM and 70% acts as the input signal for the BDFA. A 99/1 coupler at the output of the BDFA is used for the simultaneous measurements of the optical spectrum with an optical spectrum analyzer (OSA) and the optical power with another PM. A total of 99% of the output power is used for the pump power measurement, and 1% tap is used for the spectra measurements.

To determine the optical gain G, the amplified signal power P_s^{out} is calculated from the total output power P_{PM}^{out}, taking into account that it makes up a fraction f of the total output power spectrum measured at the PM, which also contains unabsorbed pump radiation and amplified spontaneous emission. Moreover, the contribution of the output coupler includes its coupling ratio R_{out}. The wavelength-dependent gain $G(\lambda)$ is obtained as the ratio of the signal output power to its input power, P_s^{in},

$$G(\lambda) = 10 \cdot \log_{10}\left(\frac{P_{PM}^{out}(\lambda) \cdot f(\lambda) \cdot R_{out}(\lambda)}{P_{PM}^{in}(\lambda) \cdot R_{in}(\lambda)}\right), \quad (1)$$

where P_s^{in} is determined with readings of the corresponding PM (P_{PM}^{in}) taking into account the coupling ratio of the input coupler, R_{in}.

The noise figure (NF) is determined using the noise subtraction technique,[32]

$$NF(\lambda) = 10\log_{10}\left(\frac{\rho_{noise}(\lambda)}{G(\lambda)h\nu} + \frac{1}{G(\lambda)}\right), \quad (2)$$

where ρ_{noise} is the noise spectral density at the output of the amplifier, h is Planck's constant, and ν is the frequency of the signal radiation. The input noise is negligible as compared to other sources of noise due to a high signal-to-noise ratio at the input (>70 dB). The spectral noise level at the signal wavelength is determined from the optical spectrum, and the noise spectral density is calculated by taking into account the total output power measured by PM. It should be noted that the noise spectral power density depends on the input signal power, pump power, and signal wavelengths. Thus, it is determined independently for every individual measurement.

III. RESULTS

A. Performance of the BDFA

First, we characterize the performance of the developed BDFA in the bi-directional PS for seven different signal powers from −25 to 5 dBm in steps of 5 dBm. The magnitudes of G and NF for the bi-directional PS and seven different signal levels are shown in Fig. 2, while the main characteristics are summarized in Table I. Figure 2(a) shows the recorded spectra of G for different input signal powers at a total pump power of 1 W, split equally between the directions. The amplifier features a maximum gain of 39.8 dB for −25-dBm input signal power, substantially decreasing to 20.8 dB for 5-dBm input signal power. On the other hand, the corresponding 3-dB gain bandwidth increases from 30.9 to 73.6 nm with an increase in the input signal power. Figure 2(b) shows the NF spectra for the seven different input signal powers. The minimal NF of 4.6 dB is achieved with −25-dBm signal power. The minimum NF rises up to 5.3 dB with the increase in input signal power to 5 dBm. The NF magnitude rises almost linearly with a decrease in the wavelength, substantially increasing at shorter wavelengths. It is worth noting that the NF flattens from 1470 nm. The same behavior was observed in our previous work[17] being mostly pronounced with backward and bi-directional pumping.
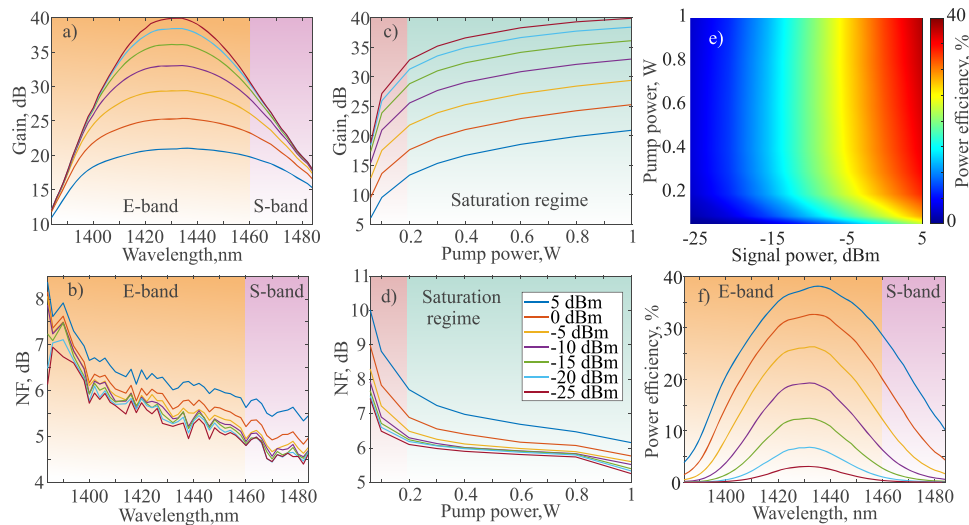

FIG. 2. Spectral dependencies of the BDFA gain (a) and NF (b) at the pump power of 1 W; the dependencies of the gain (c) and NF (d) at 1430 nm on the pump power; (e) color map of the PCE relative to the input signal and pump powers; and (f) spectra of the power efficiencies.

TABLE I. Gain and NF for the bi-directional PS with 1 W pump power and seven different signal levels.

P_{in} (dBm)	Gain (dB)	Bandwidth (nm)	NF (dB)	PCE (%)
−25	39.8	30.9	4.6	3.6
−20	38.3	34.5	4.6	7.6
−15	35.9	39.2	4.7	13.2
−10	32.9	45.2	4.8	19.6
−5	29.2	53.3	4.9	26.3
0	25.7	27.7	5	32.6
5	20.8	73.6	5.3	38

FIG. 3. (a) 1% tap spectra at the output of the amplifier for different input signal powers and (b) schematics of the gain and NF measurements.

The measured dependencies of G and NF on the pump power for the range of input signal power described above are qualitatively similar in the whole investigated spectral range of 1385–1485 nm. Therefore, only the measurements for the single wavelength of 1430 nm are presented here, as shown in Figs. 2(c) and 2(d). A gradually saturated rise of the gain magnitude and a gradually saturated reduction of the NF with an increase in the pump power are observed. The minimal pump power of 50 mW still achieves 5-dB gain for the 5-dBm signal and 20-dBm gain for the −25-dBm signal. In this case, NF is substantially higher, with 10 dB for the 5-dBm signal and 7.5 dB for the −25-dBm signal.

An important (critically important for some applications) parameter of an optical amplifier is the optical PCE. To determine the PCE, the portion of the total output optical power corresponding to the amplified signal P_s^{out} is determined from the output optical spectrum and PM, as described previously. The PCE is determined as the ratio between P_s^{out} and the total optical pump power. The measured PCE dependence on both the pump power and the input signal power at 1430 nm is represented as the color map shown in Fig. 2(e). The maximum PCE is 38%, which, to best of our knowledge, is the highest value for optical communication-compatible Bi-doped fiber amplifiers reported to date. This value is observed at the maximum pump and signal powers of 1 W and 5 dBm, respectively. The PCE clearly saturates at the pump power of 250 mW. The spectral dependence of the PCE for different input signals is also presented in Fig. 2(f). A decrease in the input signal power leads to the significant decrease in the PCE down to just 3.6% for a −25-dBm signal, as the ratio of the amplified spontaneous emission (ASE) noise power to the signal power becomes noticeably higher. To demonstrate this effect, Fig. 3(a) shows the 1% tap spectra at the output of the amplifier, including the amplified 1430 nm signal along with the ASE noise generated in the amplifier for a different input signal power at 1 W of pump power. The spectra are recorded after. The ratio of the ASE generated in the amplifier grows significantly with the decrease in the input signal power, which also leads to a decrease in the output power of the signal. This effect is explained by the lower rate of interaction between small signal and bismuth active centers. Additionally, we present the spectra of the calculated portion of the signal power (excluding the pump power and ASE) to the total output power shown in Fig. 3(b). The portion of the total output power devoted to the signal decreases with the decrease in the input signal power. Such a decrease can also be seen when the signal wavelength moves further away from the peak gain.
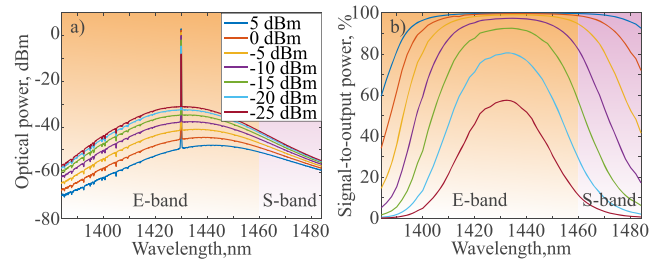
We would like to emphasize that without imposing the requirement of telecom-compatibility, the power conversion efficiency can be increased further, to about 60% for E-band BDFA; see Ref. 33 However, this further power conversion efficiency would require changes, making the amplifier not suitable for optical communications application due to two main reasons. The first issue is that the amplifier considered in Ref. 33 does not have an output isolator required to provide protection from any back-scattered signal in the line and a pump blocker at the output amplifier, leading to the pump radiation leaking to the transmission fiber, which is unsuitable for optical communications. The second issue with a further increase in PCE is that it would require high signal power. For instance, in Ref. 33, high PCE was achieved for the amplifier operating in the saturation regime (high signal power of 15 dBm), where the amplifier provides a very low gain (8 dB).

B. Pumping scheme comparison

As the next step, we investigate the performance of different PSs. As the dependencies of G and NF on the variation of pump and signal power have a behavior similar to that of the bi-directional case, we present the measurements only for three input signal powers of −25, −10, and 5 dBm. The pump power for all three PSs (bi-directional, forward, and backward) is fixed to be 500 mW. In the case of bi-directional pumping, the forward and backward pump powers are equal to 250 mW each. The comparison of different PSs in terms of G and NF for 5 dBm input signal power is presented in Figs. 4(a) and 4(b), while the main characteristics are listed in Table II. The gain spectra for all PSs are quite similar in shape, except for the bi-directional pumping, which has a slightly higher optical gain at a shorter wavelength. The backward PS shows the marginally highest gain of 17.8 dB at an input signal power of 5 dBm. On the other hand, the bi-directional PS features the marginally highest 3-dB gain bandwidth of 80.2 nm.

Even though the backward PS produces the minimum NF of 5.21 dB at 1480 nm, the main part of the NF spectra (1384–1460 nm) lies higher than in the other PSs (marked green). The wavelength is 1460 nm where all three graphs meet and start following significantly different trends. If the curves on the left-hand side of the spectra are positioned from forward, bi-directional to backward (from bottom to top), then on the right-hand side of the spectra, the curves are in the following order: backward, bi-directional, and forward (from bottom to top). Such a trend can be explained by the emergence of four-wave mixing (FWM) components that occur due to the
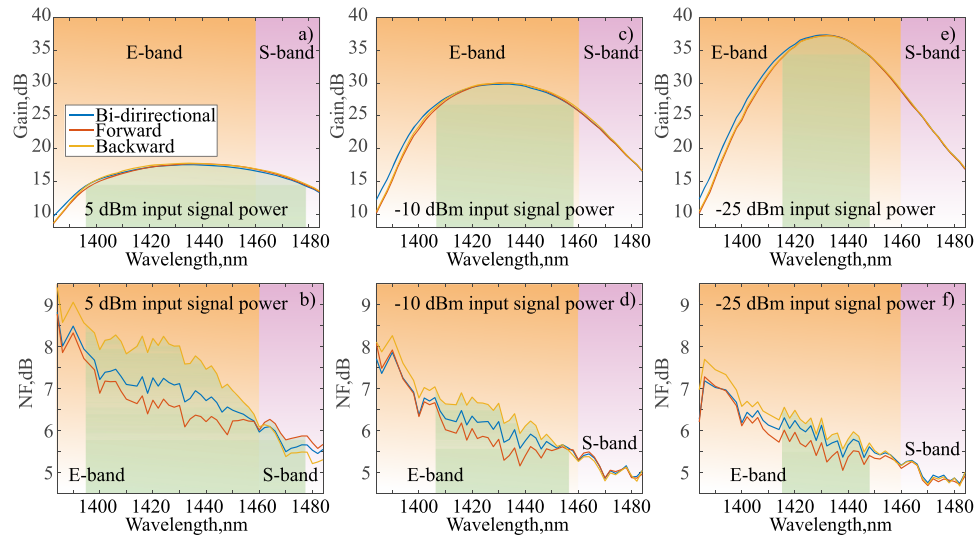
FIG. 4. Spectral dependence of the gain and NF for input signal powers of 5-dBm (a) and (b), −10-dBm (c) and (d), and −25-dBm (e) and (f). The green area under the graphs shows an approximate area of 3 dB gain bandwidth.

transfer of the pump modes toward the signal. This effect is explained in detail in Sec. IV. It is important to note that the best overall performance in terms of NF is achieved with forward PS.

In addition to the graphical comparison of different PSs in terms of G and NF, we compare different parameters of the different PSs presented in Table II. For 5 dBm input signal power, the highest bandwidth is achieved with bi-directional PS [also obvious from Fig. 4(a)]. On the other hand, the highest PCE of 37.9% is achieved with backward PS, along with the highest G. The measurement method of the amplifier parameters has been analyzed in terms of the measurement accuracy, and the real values of the amplifier parameters can be obtained with the following accuracy: gain ±0.1 dB, NF ±0.2 dB, and bandwidth ±0.5 nm.

TABLE II. Comparison of the main amplifier characteristics for different pumping schemes and signal powers with total pump power of 0.5 W. G: gain, fw: forward, bw: backward, bi-dir: bi-directional, Bdw: bandwidth, and PCE: power conversion efficiency.

P_{in} (dBm)	Pump	G (dB)	Bdw (nm)	NF (dB)	PCE (%)
	fw	37.3	31.6	4.7	3.5
−25	bw	37.2	32.1	4.7	3.5
	bi-dir	37.4	32.8	4.7	3.6
	fw	30	46.6	4.9	20.1
−10	bw	30	48.5	4.8	20.2
	bi-dir	29.9	49.3	4.9	19.4
	fw	17.7	77.6	5.6	37.3
5	bw	17.8	79.7	5.2	37.9
	bi-dir	17.55	80.2	5.4	36

The spectra of G and NF for an input signal power of −10 dBm for different PSs are presented in Figs. 4(c) and 4(d). The maximum G for all PSs significantly increases at lower signal powers of up to 30 dB, which is the maximum value among all three of them and is achieved with backward PS. The G, in general, keeps its tendency to be more pronounced at lower wavelengths in the bi-directional PS, and the highest bandwidth is 49.3 nm. The minimal NF of 4.8 dB is achieved for backward PS. However, the difference with other PSs is only of the order of tenth of a dB, which is comparable to the accuracy of the measurement methodology. Moreover, the NF spectral performance keeps its trend with a lower NF for forward pumping in the center and long wavelength regions of the operation bandwidth (highlighted in green in Fig. 4). The red part of the spectrum features almost equal values of NF for all three PSs. The achieved PCE for −10 dBm input signal power are 20.2%, 20.1%, and 19.4% for backward, forward, and bi-directional PSs, respectively.

Finally, we present the comparison of G and NF for −25-dBm input signal power and different PSs shown in Figs. 4(e) and 4(f). The maximum gain is achieved with the bi-directional PS and is equal to 37.35 dB. However, other PSs show similar gains of 37.3 and 37.2 dB for forward and backward PSs, respectively. For low signal power, the bi-directional PS enables the widest bandwidth of 32.8 nm and a similar shape to 5 dBm and −10 dBm signal powers. The NF dependence on wavelength follows a similar trend as in the case of −10 dBm signal power, with even lower differences between PSs, forward pumping being the lowest over almost the whole spectrum. The lowest NF of 4.7 dB is achieved for all pumping schemes. The small difference in the minimal NF shows an insignificant advantage of forward PS because the overall performance in the operating regimes (1410–1460 nm) for all PSs is quite similar with minimal improvement in the forward PS. The highest PCE of 3.6% is featured by bi-directional pumping, followed by 3.5% for forward pumping and 3.46% for backward PS.
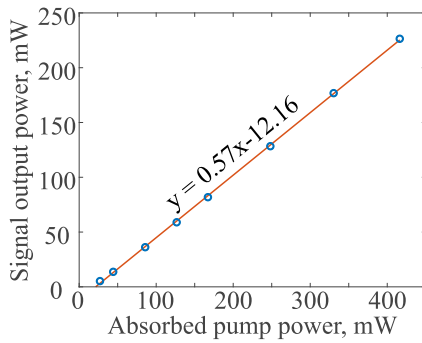
FIG. 5. Power conversion efficiency of the fiber.

C. Quantum efficiency

As the final step, the quantum efficiency of the fiber is determined for the backward pumping scheme. The quantum efficiency is an important parameter that shows the ratio of the pump photons converted into photons at the signal wavelengths to the total amount of the photons emitted in the active fiber. Measurements similar to those described in Sec. II are performed by measuring the signal output and input power and signal optical spectrum. However, an additional measurement is performed to measure the unabsorbed pump power. The input signal power of the amplifier is 10 dBm, and the wavelength of the signal is 1430 nm. Then, the dependency of the output signal power (including loss on the output TFF-WDM, isolator, and connector of 0.3, 0.42, and 0.15 dB, respectively) is plotted against the absorbed pump power (also calculated using the TFF-WDM, isolator, and connector loss). This dependency is shown

in Fig. 5. The slope of the curve of the output power to the absorbed pump power is the maximum attainable power efficiency of the active fiber. In the case of the used BDF, the slope efficiency is 57%. Quantum efficiency of the fiber can be easily obtained by multiplying the slope efficiency by the ratio between the pump frequency to signal frequency, which equals 1.075 for 1430 nm signal wavelength and 1330 nm pump wavelength. Thus, the quantum efficiency of the fiber is 61%.

It is important to highlight that looking over all input signal powers, the most favorable PS in terms of the achieved NF is the forward PS due to a generally better performance in the operational bandwidth and in the region specifically close to the gain maximum. Another remark should be made regarding the achieved PCE of 38%, which is the record value for Bi-doped fiber amplifiers, to the best of our knowledge. The high PCE achieved in this work indicates significant progress in the manufacture of BDFs. Even more important is that this magnitude is almost double the typical PCE of L-band EDFAs of around 20%.[34] However, it is still lower than the PCE of C-band EDFAs with around 50% PCE.[35] However, such a high PCE, along with 40 dB gain and 4.6 dB NF, shows a great potential for BDFAs for extension of the current infrastructure bandwidth, while keeping the power consumption at a low level.

IV. DISCUSSION

A. Four-wave mixing process

As indicated in Subsection III B, a peculiar performance of NF in the longer wavelength region has been observed, wherein the NF for the backward PS is better than that for the forward PS, contradicting the classical performance of doped-fiber amplifiers.
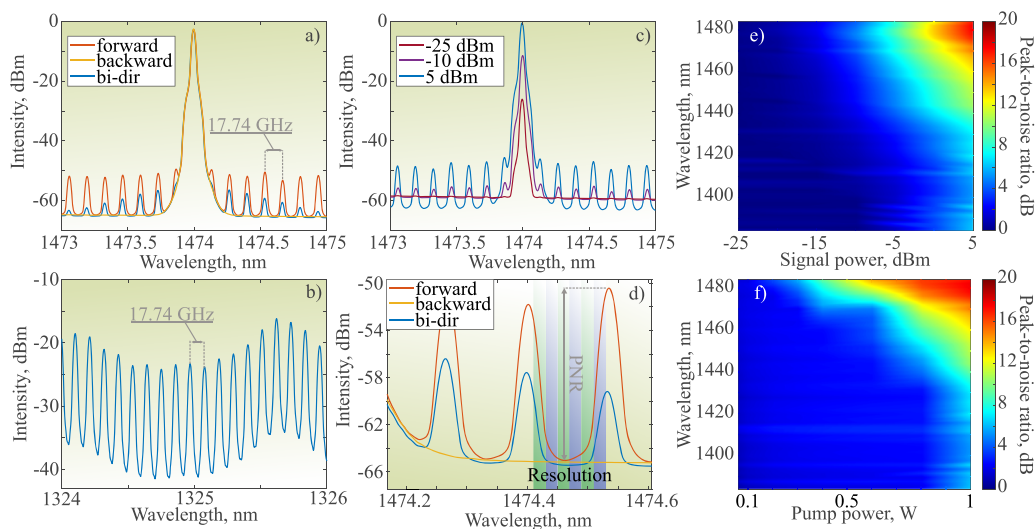

FIG. 6. Comparison of the impact of FWM on the signal spectra for forward, backward, and bi-directional pumping schemes for a signal at 1474 nm (a); the modes of the used pump laser (b); a comparison of the signal spectra for −25 dBm, −10 dBm, and 5 dBm input signal power (c); magnification of the comparison shown in (a) for wavelength range of 1474.2–1474.6 nm (d); color map of the peak-to-noise ratio relative to the wavelength and signal power for forward PS and fixed pump power of 1 W (e); and color map of the peak-to-noise ratio relative to the wavelength and pump power for forward PS and fixed input signal power of 5dBm (f).

This classical performance can be observed in the whole wavelength region from 1384 to 1460 nm, where the forward PS shows a better NF performance. However, starting from 1460 nm and toward a higher wavelength, the NF for the backward PS is better for both bi-directional and forward pumping schemes, especially for higher input signal powers.

To investigate this observation further, the detailed spectra of the signal for all three PSs were compared to identify the cause of this behavior. This comparison for a 5 dBm signal at 1474 nm is presented in Fig. 6(a). Here, it is evident that there are sub-peaks arising in the spectrum diverging from the main peak for the forward and bi-directional PSs, unlike the backward PS. Moreover, the peaks are less pronounced in the case of the bi-directional PS compared to the forward PS. The spacing between the sub-peaks is 17.74 GHz, which corresponds to the separation of sub-peaks of the pump laser diode shown in Fig. 6(b). These numerous spectral modes of the pump diode arise mostly due to two facts: the diode has a non-single-frequency, and its emission wavelength is close to the zero dispersion wavelength of SMF where it is transmitted (1310 nm), which leads to FWM broadening of the spectrum. Both of these factors lead to FWM broadening of the diode spectra by multiplication of spectral modes of the pump laser in the SMF, where it is transmitted to the amplifier. Due to multiple possible combinations of interactions and different fibers involved, it is challenging to describe the exact schematic of the created side bands; however, the majority of them arise from pump–signal–pump interaction. A detailed study with a schematic representation of the possible FWM products and interactions between the signal and the pump are presented in the paper by Gordienko et al.[36] If we change the input signal power to the amplifier, the side peaks are also reduced [shown in Fig. 6(c)]. This spectral mode transfer from lower wavelengths to higher wavelengths can happen due to the FWM process occurring between modes of the pump and the amplified signal. To quantify the effectiveness of the FWM process, we calculated the peak-to-noise ratio (PNR), a value that determines the ratio between the highest sub-peak and the noise floor. An example of this value is shown in Fig. 6(d) based on the magnification of Fig. 6(a) in the vicinity of 1474.2 and 1474.6 nm. It should be noted that Fig. 6 also shows the minimal resolution of the spectrometer that is recorded in relation to the sub-peaks. The resolution window is small enough to determine the sub-peak structure. However, it might not be good enough to determine the real minima between the sub-peaks. That might lead to variation in the calculated NF and small errors when determining the PNR. The color maps of the recorded PNR for different wavelengths, pump, and signal powers are shown in Figs. 6(e) and 6(f). The side peaks become most pronounced for wavelengths longer than 1440 nm, and the relative input signal power threshold for them to arise is between −10 and −5 dBm. In the case of pump power, side peaks appear at quite a low pump power of 0.25 W for 1480 nm. The structure of the output spectrum shown in Figs. 6(a), 6(c) and 6(d) and the relative broadband (1430–1480 nm) of effective interaction between the signal and the pump show that the zero dispersion wavelength of the bismuth fiber is around 1390–1410 nm and might change throughout the length of the fiber, which leads to the phase-matching conditions for the effective FWM process between the pump and signal. This relative estimation of the zero dispersion wavelength can be expected from the waveguide with such a core diameter and concentration of germanium.
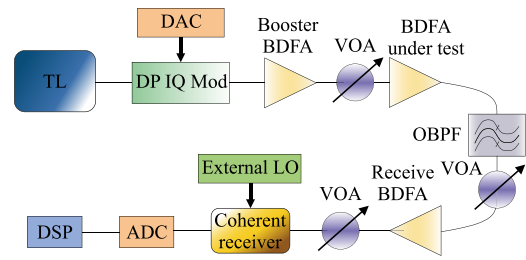

FIG. 7. Experimental setup for comparison of the impact of different pumping schemes on the transmitted signal quality.

B. Impact of four-wave mixing on the quality of data transmission

As the observed FWM process can influence the quality of transmission, experimental verification of this impact or lack of such is required. Typically, the transmitted power per channel of the signal is between −5 and 0 dBm at the input to the line, leading to −25 to −15 dBm input signal power per channel after transmission through 50–80 km of SMF with an average loss of 13–20 dB in the E-band. However, here, we perform the measurements with a higher input single power between −10 and 4 dBm.

To perform a comparison between different pumping schemes and determine the impact of four-wave mixing on the signal quality, a simple experiment of back-to-back transmission of 30 GBaud 16-QAM signal is designed. The experimental setup of the transceiver is shown in Fig. 7. The data carrier signal is generated using a TL operating from 1380 to 1480 nm, which is modulated by a dual-polarization IQ modulator (DP IQ Mod) driven by a digital-to-analog converter (DAC) to achieve DP 30 GBaud 16-QAM modulation. The signal after the modulator is amplified by the booster due to the high loss of the DP IQ modulator. The booster amplifier is the BDFA reported in the paper[17] with backward propagating pumping to allow FWM-free amplification and, thus, to minimize the possible impact of the booster amplifier on the signal quality. A variable optical attenuator (VOA) is used to control the launched signal power to the BDFA under test. The input signal power is changed in the range of −10 dBm to 4 dBm at 1430 nm (FWM-free case) and 1480 nm (FWM case). If FWM impacts the performance of the amplifier, then one can expect a degradation of forward and bi-directional pumping schemes in comparison to backward pumping schemes with increases in launch power.

After the BDFA under test, the optical bandpass filter (OBPF) is used to filter out the data carrier from ASE generated in the two amplifiers. The filter was set to the maximum bandwidth of 120 GHz to allow the data carrier to fully pass the filter along with some noise around it. The use of the OBPF is crucial to enable the receiver amplifier to provide gains predominant to the data carrier. Another VOA also controls the power at the input to the receive BDFA to enable the constant performance of this amplifier throughout the power sweep and pump scheme variation. The input power to the receiver amplifier is fixed to −10 dBm. After amplification, the data carrier power is controlled with another VOA to be 8 dBm (due to the limitations of the coherent receiver). An attenuated signal is detected by a coherent receiver, where it is combined with an

08 April 2024 16:24:09
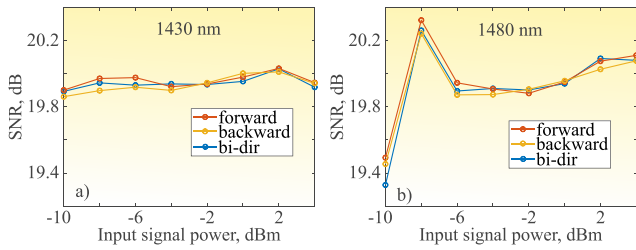
FIG. 8. SNR performance comparison for backward, forward, and bi-directional pumping schemes of the transmitted 30 GBaud 16 QAM signal at 1430 nm (a) and 1480 nm (b).

external local oscillator (LO). An analog-to-digital converter (ADC) and digital signal processing (DSP) enable the signal decoding.

The power sweep comparison between the performance of the three pumping schemes in terms of the signal-to-noise ratio (SNR) at 1430 and 1480 nm is presented in Fig. 8. The pump power for all pumping schemes is kept constant and equal to 500 mW. For small input signal powers ($< −4$ dBm for 1430 nm and $< −2$ dBm for 1480 nm), the best performing PS is the forward PS for both the wavelengths. With the increase in the input signal power, there is no clear difference between the PSs and their relative performance change from data point to data point. The similarity of data points indicates that there is no significant impact on the quality of the signal from the amplifier at high input signal powers. Even though there is no impact on the performance of coarsely spaced channels, FWM in a dense WDM system should be tested with care. This work is beyond the scope of our study and will be presented in the future.

C. Performance comparison

Finally, we would like to compare the performance of the developed BDFA in this work with other BDFAs reported in the literature. The summarized comparison between some of the highlighted studies is presented in Table III. First, we would like to stress that different input signal powers are often used for characterization of the amplifiers in the literature, and thus, the comparison is limited in that regard. Consequently, the table includes the value of the input signal power that the amplifier parameter was measured with. The target of this work was to design and comprehensively investigate a telecom-grade BDFA, and thus, first of all, we will

compare other amplifiers based on the possibility of their utilization in optical communication links. The recent work from Southampton Optic Research Center (SORC) by Wang et al.[37] has shown impressive results in terms of the gain achieved per meter, NF. However, the developed amplifier has quite a low (24 dB) small signal gain and was only studied comprehensively at low input signal powers. Nonetheless, the fiber presented in the work is capable of providing a higher gain provided with longer lengths.

The first demonstration of the cladding-pumped BDFA was presented in the paper by Vakrushev et al.[38] Unfortunately, the paper does not state the level of the input signal power; however, based on the average characteristics of other amplifiers, it can be assumed that the amplifier was characterized with a small signal. The amplifier features average characteristics for BDFA with 32 dB peak gain, 40 nm bandwidth, and 5.5 dB NF. The PCE of the amplifier is significantly lower than those of the core-pumped amplifiers; however, cladding-pumping provides a power-consumption benefit of using cooling without a power hungry thermo-electric cooler.

Another paper from the Dianov Fiber Optic Research Center (FORC)[26] presents a wideband BDFA that covers an impressive 125 nm bandwidth. However, as the fiber used in the work is phosphosilicate, the performance within the E-band is worse compared to that of germanosilicate BDFAs. For instance, the gain falls down significantly after 1450 nm, and the NF is quite high compared to the average performance, peaking at $≈7$ dB at 1430 nm. The paper reports a quite high 22% PCE with 13 dBm input signal power.

The recent paper by Liu et al.[39] from the Wuhan National Laboratory for Optoelectronics reported a high gain per meter and high small signal gain (39.2 dB) amplifier. The paper provides the analysis of only small signal performance, and thus, it is not clear how good the developed amplifier will behave with typical telecommunication input signal powers of $≈0$ dBm. The paper reports a high PCE of 13% at the small signal power of $−20$ dBm. Additionally, the amplifier is pumped at the peak of absorption that leads to a significantly higher minimal NF of 5.5 dB.

Finally, the amplifier developed at Dianov FORC and reported in the paper by Melkumov et al.[33] shows an impressive 60% PCE with 12 dBm input signal power. Such high PCE is explained by the following two main factors: (1) the design of the amplifier does not include output isolator and WDM, which leads to the pump from the amplifier to be leaked into the transmission line and the back scattered radiation from the line to be returned into the amplifier and (2) the measurements are performed with high input signal

TABLE III. Comparison of the recently reported E-band BDFAs. The compared parameters are presented for peak values, except the NF with the minimal value. The input signal power is indicated in brackets in dBm.

References	Gain (dB)	Bandwidth (nm)	NF (dB)	PCE (%)	Length (m)	Notes
This work	39.8 (−25)	73.6 (5)	4.6 (−25)	38 (5)	173	···
Wang et al.[37]	24 (−30)	≈50(−10)	4 (−30)	3.5 (−5)	35	High gain per meter, low PCE
Vakhrushev et al.[38]	32	40	5.5	≈0.01	200	Cladding pump
Ososkov et al.[26]	33 (−25)	125 (−25)	5.5 (−25)	22 (13)	150	Phosphosilicate
Liu et al.[39]	39.2 (−20)	≈40(−20)	5.5 (−20)	13(−20)	45	Pump at peak of absorption
Melkumov et al.[33]	35 (−20)	30 (−20)	6 (−20)	60 (12)	125	Non-telecom compatible

powers of 12 dBm, which are too high for telecommunication applications.

V. CONCLUSION

Power consumption and efficiency are key parameters of optical amplifiers that are critically important in WDM optical networks. In some applications, for instance, undersea system operation, limited electrical power is available and power efficiency becomes especially acute. Here, we report an E-band Bi-doped fiber amplifier based on 173 m long Bi-doped fiber with a simple single-stage and single-pass design. Despite this simplicity, the amplifier demonstrates a record gain of 39.8 dB and a record power conversion efficiency of 38% for an optical communication-compatible E-band BDFA. The achieved minimal NF is 4.7 dB, which is also the lowest reported value for single-pass Bi-doped fiber amplifiers operating in E- and S-bands. The power conversion efficiency achieved is twice as high as compared to L-band EDFAs and comparable to C-band EDFAs. The demonstrated performance of the newly developed BDFA indicates its excellent potential for multi-band transmission networks and provides additional evidence that a Bi-doped fiber amplifier is an outstanding candidate for the expansion of optical telecommunication capacity.

AUTHOR DECLARATIONS

Conflict of Interest

The authors have no conflicts to disclose.

Author Contributions

Aleksandr Donodin: Conceptualization (lead); Formal analysis (lead); Investigation (lead); Methodology (equal); Validation (equal); Visualization (lead); Writing – original draft (lead); Writing – review & editing (equal). **Egor Manuylovich**: Conceptualization (supporting); Formal analysis (supporting); Investigation (supporting); Methodology (equal); Validation (equal); Visualization (supporting); Writing – original draft (supporting); Writing – review & editing (equal). **Vladislav Dvoyrin**: Conceptualization (supporting); Investigation (supporting); Methodology (supporting); Resources (supporting); Supervision (supporting); Validation (supporting); Writing – review & editing (supporting). **Mikhail Melkumov**: Methodology (supporting); Resources (equal); Supervision (supporting); Writing – review & editing (equal).

Valery Mashinsky: Methodology (supporting); Resources (equal); Supervision (supporting); Writing – review & editing (equal). **Sergei Turitsyn**: Conceptualization (supporting); Funding acquisition (lead); Resources (lead); Supervision (lead); Writing – original draft (supporting); Writing – review & editing (lead).

DATA AVAILABILITY

The data that support the findings of this study are available from the corresponding author upon reasonable request.

REFERENCES

[1] P. J. Winzer, D. T. Neilson, and A. R. Chraplyvy, "Fiber-optic transmission and networking: The previous 20 and the next 20 years [Invited]," Opt. Exp. **26**, 24190–24239 (2018).

[2] T. Fehenberger, A. Alvarado, G. Böcherer, and N. Hanik, "On probabilistic shaping of quadrature amplitude modulation for the nonlinear fiber channel," J. Lightwave Technol. **34**, 5063–5073 (2016).

[3] A. D. Ellis, J. Zhao, and D. Cotter, "Approaching the non-linear Shannon limit," J. Lightwave Technol. **28**, 423–433 (2010).

[4] A. Ferrari, A. Napoli, J. K. Fischer, N. Costa, A. D'Amico, J. Pedro, W. Forysiak, E. Pincemin, A. Lord, A. Stavdas *et al.*, "Assessment on the achievable throughput of multi-band ITU-T G.652.D fiber transmission systems," J. Lightwave Technol. **38**, 4279–4291 (2020).

[5] L. Rapp and M. Eiselt, "Optical amplifiers for multi–band optical transmission systems," J. Lightwave Technol. **40**, 1579–1589 (2022).

[6] T. Hoshida, V. Curri, L. Galdino, D. T. Neilson, W. Forysiak, J. K. Fischer, T. Kato, and P. Poggiolini, "Ultrawideband systems and networks: Beyond C + L-band," Proc. IEEE **110**, 1725–1741 (2022).

[7] J. Renaudier, A. Napoli, M. Ionescu, C. Calo, G. Fiol, V. Mikhailov, W. Forysiak, N. Fontaine, F. Poletti, and P. Poggiolini, "Devices and fibers for ultrawideband optical communications," Proc. IEEE **110**, 1742–1759 (2022).

[8] M. A. Iqbal, L. Krzczanowicz, I. Phillips, P. Harper, and W. Forysiak, "150nm SCL-band transmission through 70km SMF using ultra-wideband dual-stage discrete Raman amplifier," in *Optical Fiber Communication Conference* (Optical Society of America, 2020), pp. W3E–W4.

[9] J. Renaudier, A. Arnould, A. Ghazisaeidi, D. L. Gac, P. Brindel, E. Awwad, M. Makhsiyan, K. Mekhazni, F. Blache, A. Boutin *et al.*, "Recent advances in 100 + nm ultra-wideband fiber-optic transmission systems using semiconductor optical amplifiers," J. Lightwave Technol. **38**, 1071–1079 (2020).

[10] M. Stephens, V. Gordienko, and N. Doran, "20 dB net-gain polarization-insensitive fiber optical parametric amplifier with >2 THz bandwidth," Opt. Express **25**, 10597–10609 (2017).

[11] A. Sobhanan, A. Anthur, S. O'Duill, M. Pelusi, S. Namiki, L. Barry, D. Venkitesh, and G. P. Agrawal, "Semiconductor optical amplifiers: Recent advances and applications," Adv. Opt. Photonics **14**, 571–651 (2022).

[12] C. D. Boley, J. W. Dawson, L. S. Kiani, and P. H. Pax, "E-Band neodymium-doped fiber amplifier: Model and application," Appl. Opt. **58**, 2320–2327 (2019).

[13] L. Chorchos and J. P. Turkiewicz, "Experimental performance of semiconductor optical amplifiers and praseodymium-doped fiber amplifiers in 1310-nm dense wavelength division multiplexing system," Opt. Eng. **56**, 046101 (2017).

[14] S. Chen, Y. Jung, S.-u. Alam, D. J. Richardson, R. Sidharthan, D. Ho, S. Yoo, and J. M. Daniel, "Ultra-short wavelength operation of thulium-doped fiber amplifiers and lasers," Opt. Exp. **27**, 36699–36707 (2019).

[15] Y. Wang, N. K. Thipparapu, D. J. Richardson, and J. K. Sahu, "Ultra-broadband bismuth-doped fiber amplifier covering a 115-nm bandwidth in the O and E bands," J. Lightwave Technol. **39**, 795–800 (2021).

[16] I. A. Bufetov, M. A. Melkumov, S. V. Firstov, K. E. Riumkin, A. V. Shubin, V. F. Khopin, A. N. Guryanov, and E. M. Dianov, "Bi-doped optical fibers and fiber lasers," IEEE J. Sel. Top. Quantum Electron. **20**, 111–125 (2014).

[17] A. Donodin, V. Dvoyrin, E. Manuylovich, L. Krzczanowicz, W. Forysiak, M. Melkumov, V. Mashinsky, and S. Turitsyn, "Bismuth doped fibre amplifier operating in E- and S-optical bands," Opt. Mater. Express **11**, 127–135 (2021).

[18] V. Mikhailov, J. Luo, D. Inniss, M. Yan, Y. Sun, G. S. Puc, R. S. Windeler, P. S. Westbrook, Y. Dulashko, and D. J. DiGiovanni, "Amplified transmission beyond C-and L-bands: Doped fibre amplifiers for 1250–1450 nm range," in *2020 European Conference on Optical Communications (ECOC)* (IEEE, 2020), pp. 1–3.

[19] V. Dvoyrin, V. M. Mashinsky, and S. Turitsyn, "Bismuth-doped fiber amplifier operating in the spectrally adjacent to EDFA range of 1425-1500 nm," in *Optical Fiber Communication Conference* (Optica Publishing Group, 2020), p. W1C-5.

[20] M. A. Melkumov, V. Mikhailov, A. M. Khegai, K. E. Riumkin, S. V. Firstov, F. Afanasiev, A. N. Guryanov, M. Yan, Y. Sun, J. Luo *et al.*, "25 Gb s^{-1} data transmission using a bismuth-doped fibre amplifier with a gain peak shifted to 1300 nm," Quantum Electron. **48**, 989 (2018).

[21] Y. Wakayama, D. J. Elson, V. Mikhailov, R. Maneekut, J. Luo, N. Yoshikane, D. Inniss, and T. Tsuritani, "400GBASE-LR4 and 400GBASE-LR8 transmission reach maximization using bismuth-doped fiber amplifiers," J. Lightwave Technol. **41**, 3908–3915 (2023).

[22] M. Melkumov, V. Mikhailov, A. Hegai, K. Riumkin, P. Westbrook, D. DiGiovanni, and E. Dianov, "E-band data transmission over 80 km of non-zero dispersion fibre link using bismuth-doped fibre amplifier," Electron. Lett. **53**, 1661–1663 (2017).

[23] A. Donodin, V. Dvoyrin, E. Manuylovich, I. Phillips, W. Forysiak, M. Melkumov, V. Mashinsky, and S. Turitsyn, "4-channel E-band data transmission over 160 km of SMF-28 using a bismuth-doped fibre amplifier," in *2021 Optical Fiber Communications Conference and Exhibition (OFC)* (IEEE, 2021), pp. 1–3.

[24] A. Donodin, M. Tan, P. Hazarika, V. Dvoyrin, I. Phillips, P. Harper, S. Turitsyn, and W. Forysiak, "30-GBaud DP 16-QAM transmission in the E-band enabled by bismuth-doped fiber amplifiers," Opt. Lett. **47**(19), 5152–5155 (2022).

[25] A. Donodin, E. London, B. Correia, E. Virgillito, M. Tan, P. Hazarika, I. Phillips, P. Harper, S. K. Turitsyn, V. Curri, and W. Forysiak, "Multi-band ESCL transmission supported by bismuth-doped and Raman fiber amplification," J. Lightwave Technology (2023).

[26] Y. Ososkov, A. Khegai, S. Firstov, K. Riumkin, S. Alyshev, A. Kharakhordin, A. Lobanov, A. Guryanov, and M. Melkumov, "Pump-efficient flattop O + E-bands bismuth-doped fiber amplifier with 116 nm −3 dB gain bandwidth," Opt. Express **29**, 44138–44145 (2021).

[27] Y. Wang, N. K. Thipparapu, D. J. Richardson, and J. K. Sahu, "High gain Bi-doped fiber amplifier operating in the E-band with a 3-db bandwidth of 40 nm," in *Optical Fiber Communication Conference* (Optica Publishing Group, 2021), p. Tu1E.1.

[28] V. Dvoyrin, O. Medvedkov, V. Mashinsky, A. Umnikov, A. Guryanov, and E. Dianov, "Optical amplification in 1430–1495 nm range and laser action in bi-doped fibers," Opt. Express **16**, 16971–16976 (2008).

[29] V. Dvoirin, V. Mashinskii, O. I. Medvedkov, A. A. Umnikov, A. N. Gur'yanov, and E. M. Dianov, "Bismuth-doped telecommunication fibres for lasers and amplifiers in the 1400–1500-nm region," Quantum Electron. **39**, 583 (2009).

[30] V. Mashinsky and V. Dvoyrin, "Bismuth-doped fiber amplifiers: State of the art and future prospect," in *2009 IEEE LEOS Annual Meeting Conference Proceedings* (IEEE, 2009), pp. 775–776.

[31] A. Zlenko, V. Dvoyrin, V. Mashinsky, A. Denisov, L. Iskhakova, M. Mayorova, O. Medvedkov, S. Semenov, S. Vasiliev, and E. Dianov, "Furnace chemical vapor deposition bismuth-doped silica-core holey fiber," Opt. Lett. **36**, 2599–2601 (2011).

[32] D. M. Baney, P. Gallion, and R. S. Tucker, "Theory and measurement techniques for the noise figure of optical amplifiers," Opt. Fiber Technol. **6**, 122–154 (2000).

[33] M. Melkumov, I. Bufetov, A. Shubin, S. Firstov, V. Khopin, A. Guryanov, and E. Dianov, "Laser diode pumped bismuth-doped optical fiber amplifier for 1430 nm band," Opt. Lett. **36**, 2408–2410 (2011).

[34] L. Qian and R. Bolen, "Erbium-doped phosphosilicate fiber amplifiers: A comparison of configurations for the optimization of noise figure and conversion efficiency," *Photonic Applications in Devices and Communication Systems* (International Society for Optics and Photonics, 2005), Vol. 5970, p. 59702V.

[35] R. Laming, J. Townsend, D. Payne, F. Meli, G. Grasso, and E. Tarbox, "High-power erbium-doped-fiber amplifiers operating in the saturated regime," IEEE Photonics Tech. Lett. **3**, 253–255 (1991).

[36] V. Gordienko, M. A. Z. Al-Khateeb, F. M. Ferreira, A. D. Ellis, and N. J. Doran, "Unwanted four-wave mixing in fibre optical parametric amplifiers," in *2019 21st International Conference on Transparent Optical Networks (ICTON)* (IEEE, 2019), pp. 1–4.

[37] S. Wang, Z. Zhai, A. Halder, and J. K. Sahu, "Bi-doped fiber amplifiers in the E + S band with a high gain per unit length," Opt. Lett. **48**, 5635–5638 (2023).

[38] A. Vakhrushev, A. Khegai, S. Alyshev, K. Riumkin, A. Kharakhordin, E. Firstova, A. Umnikov, A. Lobanov, F. Afanasiev, A. Guryanov *et al.*, "Cladding pumped bismuth-doped fiber amplifiers operating in O-, E-, and S-telecom bands," Opt. Lett. **48**, 1339–1342 (2023).

[39] S. Liu, X. Yin, Z. Gu, L. He, W. Li, Y. Chen, Y. Xing, Y. Chu, N. Dai, and J. Li, "High bismuth-doped germanosilicate fiber for efficient E + S-band amplification," Opt. Lett. **49**, 314–317 (2024).

08 April 2024 16:24:09